Rapid Communications

Measurement of branching fraction and final-state asymmetry for the $\bar{B}^0 \to K^0_S K^{\mp}\pi^{\pm}$ decay

Y.-T. Lai,[17] I. Adachi,[17,13] H. Aihara,[86] S. Al Said,[80,35] D. M. Asner,[3] H. Atmacan,[76] V. Aulchenko,[4,64] T. Aushev,[54] V. Babu,[81] I. Badhrees,[80,34] A. M. Bakich,[79] V. Bansal,[66] P. Behera,[24] C. Beleño,[12] B. Bhuyan,[22] T. Bilka,[5] J. Biswal,[31] A. Bobrov,[4,64] A. Bozek,[62] M. Bračko,[48,31] L. Cao,[32] D. Červenkov,[5] P. Chang,[61] V. Chekelian,[49] A. Chen,[59] B. G. Cheon,[15] K. Chilikin,[42] K. Cho,[37] S.-K. Choi,[14] Y. Choi,[78] S. Choudhury,[23] D. Cinabro,[90] S. Cunliffe,[7] N. Dash,[21] S. Di Carlo,[40] Z. Doležal,[5] T. V. Dong,[17,13] S. Eidelman,[4,64,42] D. Epifanov,[4,64] J. E. Fast,[66] A. Frey,[12] B. G. Fulsom,[66] R. Garg,[67] V. Gaur,[89] N. Gabyshev,[4,64] A. Garmash,[4,64] M. Gelb,[32] A. Giri,[23] P. Goldenzweig,[32] D. Greenwald,[82] Y. Guan,[25,17] J. Haba,[17,13] T. Hara,[17,13] K. Hayasaka,[63] H. Hayashii,[58] W.-S. Hou,[61] C.-L. Hsu,[79] K. Huang,[61] T. Iijima,[56,55] K. Inami,[55] G. Inguglia,[7] A. Ishikawa,[84] R. Itoh,[17,13] M. Iwasaki,[65] Y. Iwasaki,[17] S. Jia,[2] Y. Jin,[86] D. Joffe,[33] A. B. Kaliyar,[24] G. Karyan,[7] T. Kawasaki,[36] H. Kichimi,[17] C. Kiesling,[49] D. Y. Kim,[75] H. J. Kim,[39] J. B. Kim,[38] S. H. Kim,[15] K. Kinoshita,[6] P. Kodyš,[5] S. Korpar,[48,31] D. Kotchetkov,[16] P. Križan,[43,31] R. Kroeger,[51] P. Krokovny,[4,64] T. Kuhr,[44] R. Kulasiri,[33] R. Kumar,[70] A. Kuzmin,[4,64] Y.-J. Kwon,[92] K. Lalwani,[46] J. S. Lange,[10] I. S. Lee,[15] J. K. Lee,[73] J. Y. Lee,[73] S. C. Lee,[39] C. H. Li,[50] L. K. Li,[26] Y. B. Li,[68] L. Li Gioi,[49] J. Libby,[24] Z. Liptak,[16] D. Liventsev,[89,17] P.-C. Lu,[61] M. Lubej,[31] T. Luo,[9] J. MacNaughton,[52] M. Masuda,[85] T. Matsuda,[52] D. Matvienko,[4,64,42] M. Merola,[28,57] K. Miyabayashi,[58] R. Mizuk,[42,53,54] G. B. Mohanty,[81] T. Mori,[55] M. Mrvar,[31] R. Mussa,[29] E. Nakano,[65] M. Nakao,[17,13] K. J. Nath,[22] M. Nayak,[90,17] N. K. Nisar,[69] S. Nishida,[17,13] S. Ogawa,[83] G. Pakhlova,[42,54] B. Pal,[3] S. Pardi,[28] H. Park,[39] S. Paul,[82] T. K. Pedlar,[45] R. Pestotnik,[31] L. E. Piilonen,[89] V. Popov,[42,54] E. Prencipe,[19] A. Rabusov,[82] M. Ritter,[44] A. Rostomyan,[7] G. Russo,[28] Y. Sakai,[17,13] M. Salehi,[47,44] S. Sandilya,[6] L. Santelj,[17] T. Sanuki,[84] V. Savinov,[69] O. Schneider,[41] G. Schnell,[1,20] C. Schwanda,[27] Y. Seino,[63] K. Senyo,[91] O. Seon,[55] M. E. Sevior,[50] C. P. Shen,[2] T.-A. Shibata,[87] J.-G. Shiu,[61] E. Solovieva,[42,54] M. Starič,[31] M. Sumihama,[11] T. Sumiyoshi,[88] W. Sutcliffe,[32] M. Takizawa,[74,18,71] K. Tanida,[30] Y. Tao,[8] F. Tenchini,[7] M. Uchida,[87] T. Uglov,[42,54] Y. Unno,[15] S. Uno,[17,13] P. Urquijo,[50] Y. Usov,[4,64] R. Van Tonder,[32] G. Varner,[16] K. E. Varvell,[79] V. Vorobyev,[4,64,42] B. Wang,[6] C. H. Wang,[60] M.-Z. Wang,[61] P. Wang,[26] X. L. Wang,[9] E. Widmann,[77] E. Won,[38] H. Yamamoto,[84] S. B. Yang,[38] H. Ye,[7] C. Z. Yuan,[26] Y. Yusa,[63] Z. P. Zhang,[72] V. Zhilich,[4,64] V. Zhukova,[42] and V. Zhulanov[4,64]

(Belle Collaboration)

[1]*University of the Basque Country UPV/EHU, 48080 Bilbao*
[2]*Beihang University, Beijing 100191*
[3]*Brookhaven National Laboratory, Upton, New York 11973*
[4]*Budker Institute of Nuclear Physics SB RAS, Novosibirsk 630090*
[5]*Faculty of Mathematics and Physics, Charles University, 121 16 Prague*
[6]*University of Cincinnati, Cincinnati, Ohio 45221*
[7]*Deutsches Elektronen–Synchrotron, 22607 Hamburg*
[8]*University of Florida, Gainesville, Florida 32611*
[9]*Key Laboratory of Nuclear Physics and Ion-beam Application (MOE) and Institute of Modern Physics, Fudan University, Shanghai 200443*
[10]*Justus-Liebig-Universität Gießen, 35392 Gießen*
[11]*Gifu University, Gifu 501-1193*
[12]*II. Physikalisches Institut, Georg-August-Universität Göttingen, 37073 Göttingen*
[13]*SOKENDAI (The Graduate University for Advanced Studies), Hayama 240-0193*
[14]*Gyeongsang National University, Chinju 660-701*
[15]*Hanyang University, Seoul 133-791*
[16]*University of Hawaii, Honolulu, Hawaii 96822*
[17]*High Energy Accelerator Research Organization (KEK), Tsukuba 305-0801*
[18]*J-PARC Branch, KEK Theory Center, High Energy Accelerator Research Organization (KEK), Tsukuba 305-0801*
[19]*Forschungszentrum Jülich, 52425 Jülich*
[20]*IKERBASQUE, Basque Foundation for Science, 48013 Bilbao*
[21]*Indian Institute of Technology Bhubaneswar, Satya Nagar 751007*
[22]*Indian Institute of Technology Guwahati, Assam 781039*
[23]*Indian Institute of Technology Hyderabad, Telangana 502285*
[24]*Indian Institute of Technology Madras, Chennai 600036*

[25]*Indiana University, Bloomington, Indiana 47408*
[26]*Institute of High Energy Physics, Chinese Academy of Sciences, Beijing 100049*
[27]*Institute of High Energy Physics, Vienna 1050*
[28]*INFN—Sezione di Napoli, 80126 Napoli*
[29]*INFN—Sezione di Torino, 10125 Torino*
[30]*Advanced Science Research Center, Japan Atomic Energy Agency, Naka 319-1195*
[31]*J. Stefan Institute, 1000 Ljubljana*
[32]*Institut für Experimentelle Teilchenphysik, Karlsruher Institut für Technologie, 76131 Karlsruhe*
[33]*Kennesaw State University, Kennesaw, Georgia 30144*
[34]*King Abdulaziz City for Science and Technology, Riyadh 11442*
[35]*Department of Physics, Faculty of Science, King Abdulaziz University, Jeddah 21589*
[36]*Kitasato University, Sagamihara 252-0373*
[37]*Korea Institute of Science and Technology Information, Daejeon 305-806*
[38]*Korea University, Seoul 136-713*
[39]*Kyungpook National University, Daegu 702-701*
[40]*LAL, Univ. Paris-Sud, CNRS/IN2P3, Université Paris-Saclay, Orsay*
[41]*École Polytechnique Fédérale de Lausanne (EPFL), Lausanne 1015*
[42]*P.N. Lebedev Physical Institute of the Russian Academy of Sciences, Moscow 119991*
[43]*Faculty of Mathematics and Physics, University of Ljubljana, 1000 Ljubljana*
[44]*Ludwig Maximilians University, 80539 Munich*
[45]*Luther College, Decorah, Iowa 52101*
[46]*Malaviya National Institute of Technology Jaipur, Jaipur 302017*
[47]*University of Malaya, 50603 Kuala Lumpur*
[48]*University of Maribor, 2000 Maribor*
[49]*Max-Planck-Institut für Physik, 80805 München*
[50]*School of Physics, University of Melbourne, Victoria 3010*
[51]*University of Mississippi, University, Mississippi 38677*
[52]*University of Miyazaki, Miyazaki 889-2192*
[53]*Moscow Physical Engineering Institute, Moscow 115409*
[54]*Moscow Institute of Physics and Technology, Moscow Region 141700*
[55]*Graduate School of Science, Nagoya University, Nagoya 464-8602*
[56]*Kobayashi-Maskawa Institute, Nagoya University, Nagoya 464-8602*
[57]*Università di Napoli Federico II, 80055 Napoli*
[58]*Nara Women's University, Nara 630-8506*
[59]*National Central University, Chung-li 32054*
[60]*National United University, Miao Li 36003*
[61]*Department of Physics, National Taiwan University, Taipei 10617*
[62]*H. Niewodniczanski Institute of Nuclear Physics, Krakow 31-342*
[63]*Niigata University, Niigata 950-2181*
[64]*Novosibirsk State University, Novosibirsk 630090*
[65]*Osaka City University, Osaka 558-8585*
[66]*Pacific Northwest National Laboratory, Richland, Washington 99352*
[67]*Panjab University, Chandigarh 160014*
[68]*Peking University, Beijing 100871*
[69]*University of Pittsburgh, Pittsburgh, Pennsylvania 15260*
[70]*Punjab Agricultural University, Ludhiana 141004*
[71]*Theoretical Research Division, Nishina Center, RIKEN, Saitama 351-0198*
[72]*University of Science and Technology of China, Hefei 230026*
[73]*Seoul National University, Seoul 151-742*
[74]*Showa Pharmaceutical University, Tokyo 194-8543*
[75]*Soongsil University, Seoul 156-743*
[76]*University of South Carolina, Columbia, South Carolina 29208*
[77]*Stefan Meyer Institute for Subatomic Physics, Vienna 1090*
[78]*Sungkyunkwan University, Suwon 440-746*
[79]*School of Physics, University of Sydney, New South Wales 2006*
[80]*Department of Physics, Faculty of Science, University of Tabuk, Tabuk 71451*
[81]*Tata Institute of Fundamental Research, Mumbai 400005*
[82]*Department of Physics, Technische Universität München, 85748 Garching*
[83]*Toho University, Funabashi 274-8510*
[84]*Department of Physics, Tohoku University, Sendai 980-8578*

[85]Earthquake Research Institute, University of Tokyo, Tokyo 113-0032
[86]Department of Physics, University of Tokyo, Tokyo 113-0033
[87]Tokyo Institute of Technology, Tokyo 152-8550
[88]Tokyo Metropolitan University, Tokyo 192-0397
[89]Virginia Polytechnic Institute and State University, Blacksburg, Virginia 24061
[90]Wayne State University, Detroit, Michigan 48202
[91]Yamagata University, Yamagata 990-8560
[92]Yonsei University, Seoul 120-749

(Received 16 April 2019; published 10 July 2019)

We report a measurement of the branching fraction and final-state asymmetry for the $\bar{B}^0 \to K^0_S K^{\mp}\pi^{\pm}$ decays. The analysis is based on a data sample of 711 fb^{-1} collected at the $\Upsilon(4S)$ resonance with the Belle detector at the KEKB asymmetric-energy e^+e^- collider. We obtain a branching fraction of $(3.60 \pm 0.33 \pm 0.15) \times 10^{-6}$ and a final-state asymmetry of $(-8.5 \pm 8.9 \pm 0.2)\%$, where the first uncertainties are statistical and the second are systematic. Hints of peaking structures are found in the differential branching fractions measured as functions of Dalitz variables.

DOI: 10.1103/PhysRevD.100.011101

Three-body charmless hadronic B decays are suppressed in the standard model (SM); the ones with an even number of kaons have a smaller decay rate compared to those with an odd number of kaons. These three-body decays proceed via $b \to u$ tree and W-exchange diagrams, as well as $b \to s, d$ penguin processes with a virtual loop. The latter provides an opportunity to search for physics beyond the SM since new heavy particles may cause deviations from SM predictions. Due to possible interference between the aforementioned diagrams, these decays are sensitive to CP violation localized in the Dalitz plane [1,2].

Previous measurements of $\bar{B}^0 \to K^0_S K^{\mp}\pi^{\pm}$ decays [3] by *BABAR* [4,5] and LHCb [6–8] found hints of structures in the low $K^-\pi^+$ and $K^-K^0_S$ mass regions with a highly asymmetric distribution in helicity angle. These studies also reported no two-body resonance decays with $\bar{K}K^*$ final states. Furthermore, the yields were not sufficient to draw firm conclusions with a Dalitz plot analysis. Similar studies on $B^+ \to K^+K^-\pi^+$ performed by Belle [9], *BABAR* [10], and LHCb [11,12] found an unexpected peak in the K^+K^- invariant mass ($M_{K^+K^-}$) as well as strong evidence for localized CP violation near $M_{K^+K^-} < 1.5$ GeV$/c^2$. Assuming the excess is due to a two-body resonance, a search for its isospin partner decaying to $K^-K^0_S$ would help elucidate the nature of the enigmatic resonance.

We report measurements of the branching fraction and final-state asymmetry of $\bar{B}^0 \to K^0_S K^{\mp}\pi^{\pm}$ decays. Using the charges of final-state particles, the latter is defined as

$$\mathcal{A} = \frac{N(K^0_S K^-\pi^+) - N(K^0_S K^+\pi^-)}{N(K^0_S K^-\pi^+) + N(K^0_S K^+\pi^-)}, \tag{1}$$

where N denotes the signal yield obtained for the corresponding final state of both B^0 and $\bar{B}^0$. Here $\mathcal{A}$ is distinct from the direct CP asymmetry ($\mathcal{A}_{CP}$); rather it is an asymmetry between the decay final states of $K^0K^-\pi^+$ and $\bar{K}^0K^+\pi^-$ where the K^0 or $\bar{K}^0$ is reconstructed as a K^0_S. We measure this quantity as it can be more precisely determined than $\mathcal{A}_{CP}$ for this decay mode. A nonzero $\mathcal{A}$ value would be an indirect manifestation of CP violation. This is the first measurement of such an asymmetry in the $\bar{B}^0 \to K^0_S K^{\mp}\pi^{\pm}$ decay. In addition, we use the ${}_s\mathcal{P}lot$ [13] method to obtain background-subtracted yields for the Dalitz variables $M_{K^-\pi^+}$, $M_{\pi^+K^0_S}$, and $M_{K^-K^0_S}$, and hence to determine their differential branching fractions. The total branching fraction is calculated by integrating the differential branching fraction. By utilizing this well-established method, we can infer the existence of an intermediate resonance and localized asymmetry in the background-subtracted Dalitz plot, as well as compare the result from this study with previous measurements [4–12].

Our measurement is based on the full data sample of 711 fb^{-1}, corresponding to 772×10^6 $B\bar{B}$ pairs, collected on the $\Upsilon(4S)$ resonance with the Belle detector [14] at the KEKB asymmetric-energy e^+e^- collider [15]. The detector components relevant for this study are a silicon vertex detector (SVD), a 50-layer central drift chamber (CDC), an array of aerogel threshold Cherenkov counters (ACC), a barrel-like arrangement of time-of-flight scintillation counters (TOF), and an electromagnetic calorimeter made of CsI(Tl) crystals. These are located inside a superconducting solenoid that provides a 1.5 T magnetic field.

Large samples of Monte Carlo (MC) events are generated with EvtGen [16] and subsequently simulated with

GEANT3 [17] with the configurations of the Belle detector. We use these samples to obtain the expected distributions of various physical quantities for signal and backgrounds, to optimize the selection criteria, and to determine the signal detection efficiency.

The selection criteria for the final-state particles in the $\bar{B}^0 \to K^0_S K^{\mp}\pi^{\pm}$ reconstruction are based on information obtained from the tracking systems (SVD and CDC) and the charged-hadron identification (PID) systems, namely the CDC, ACC, and TOF. The charged kaons and pions are required to have an impact parameter within ± 0.2 cm of the interaction point (IP) in the transverse plane, and within ± 5.0 cm along the z axis, defined as the direction opposite the e^+ beam. The likelihood values of each track for kaon and pion hypotheses (L_K and L_π) are determined from the information provided by the PID systems. A track is identified as a kaon if $L_K/(L_K + L_\pi) > 0.6$, otherwise it is treated as a pion. The efficiency for identifying a pion (kaon) is about 88% (86%), depending on the track momentum, while the probability for a pion or a kaon to be misidentified is less than 10%. The efficiency and misidentification probabilities are averaged over the momentum of final-state particles.

The K^0_S candidates are reconstructed via the $K^0_S \to \pi^+\pi^-$ decay, and the identification is enhanced by selecting on the output of a neural network (NN) [18], which combines seven kinematic variables of the K^0_S [19]. The invariant mass of the K^0_S candidate is required to be within ± 10 MeV$/c^2$ of its world average [20], which corresponds to about three times the mass resolution. The $K^0_S \to \pi^+\pi^-$ vertex fit is required to converge with a goodness-of-fit (χ^2) value less than 20.

We identify B mesons with two kinematic variables calculated in the center-of-mass (CM) frame: the beam-energy constrained $M_{\rm bc} \equiv \sqrt{E^2_{\rm beam}/c^4 - |\vec{p}_B/c|^2}$, and the energy difference $\Delta E \equiv E_B - E_{\rm beam}$, where $E_{\rm beam}$ is the beam energy, and $\vec{p}_B$ (E_B) is the momentum (energy) of the reconstructed B meson. The B candidates are required to have $M_{\rm bc} > 5.255$ GeV$/c^2$ and $|\Delta E| < 0.15$ GeV, with the signal region given by 5.272 GeV$/c^2 < M_{\rm bc} < 5.288$ GeV$/c^2$ and $|\Delta E| < 0.05$ GeV. We require a successful vertex fit for $\bar{B}^0 \to K^0_S K^{\mp}\pi^{\pm}$ candidates, where the K^0_S trajectory is included in the fit, with $\chi^2 < 100$.

About 9% of events in the data sample have more than one B candidate, and the signal events have an average of 1.1 candidates. In such cases, we select the candidate with the smallest χ^2 value from the B vertex fit. According to simulations, our best candidate selection method chooses the correct candidate in 99% of cases.

The dominant background is from the continuum $e^+e^- \to q\bar{q}(q = u, d, s, c)$ process. To suppress it, we construct a Fisher discriminant [21] from 17 modified Fox-Wolfram moments [22]. To further improve the distinguishing power, we combine the discriminant output with four more variables in an NN. These are the cosine of the angle between the reconstructed B flight direction and the z axis in the CM frame, the offset along the z axis between the vertex of the reconstructed B and the vertex formed by the remaining tracks, the cosine of the angle between the thrust axis [23] of the reconstructed B and that of the rest of the event in the CM frame, and a B meson flavor tagging quality variable. The NN is trained with signal and continuum MC samples. The NN output ($C_{\rm NN}$) ranges from -1 to 1, and it is required to be greater than 0.7. This removes 93% of the continuum background while retaining 82% of the signal. We transform $C_{\rm NN}$ to $C'_{\rm NN} \equiv \log(\frac{C_{\rm NN} - C^{\rm min}_{\rm NN}}{C^{\rm max}_{\rm NN} - C_{\rm NN}})$, where $C^{\rm min}_{\rm NN}$ is 0.7 and $C^{\rm max}_{\rm NN}$ is the maximum value of $C_{\rm NN}$.

Background events from B decays mediated via the $b \to c$ transition (generic B decays) have peaking structures in the signal region. They are mainly due to the decays with two-body final states of D and J/ψ mesons, e.g., $D^0 \to K^-\pi^+$, $D^- \to K^- K^0_S$, $D^-_s \to K^- K^0_S$, $J/\psi \to e^+e^-$, and $J/\psi \to \mu^+\mu^-$. These decays can be identified by peaks at the nominal D and J/ψ mass [20] in the distributions of the invariant masses of two of the final-state particles ($M_{K^-\pi^+}$, $M_{\pi^+ K^0_S}$, $M_{K^- K^0_S}$, where we allow for a change in the mass hypothesis of a charged kaon or pion). We exclude events within $\pm 4\sigma$ of the nominal mass of the peaking structures to suppress the contributions from D and J/ψ mesons.

The rare B background from $b \to u, d, s$ transitions is studied with a large MC sample in which the branching fractions are much larger than the measured or expected values. Two modes are found to have peaks near the ΔE signal region: $B^0 \to K^- K^+ K^0_S$ and $B^0 \to \pi^-\pi^+ K^0_S$, including their intermediate resonant modes. The remaining rare B events have a relatively flat ΔE distribution.

The signal yield and $\mathcal{A}$ are extracted from a three-dimensional extended unbinned maximum likelihood fit, with the likelihood defined as

$$\mathcal{L} = \frac{e^{-\sum_j N_j}}{N!} \prod_{i=1}^{N} \left(\sum_j N_j P^i_j \right), \tag{2}$$

where

$$P^i_j = \frac{1}{2}(1 - q^i \cdot \mathcal{A}_j) \times P_j(M^i_{\rm bc}, \Delta E^i, C'^i_{\rm NN}), \tag{3}$$

N is the number of candidate events, N_j is the number of events in category j, i is the event index, q^i is the charge of the $K^{\pm}$ in the i-th event, $\mathcal{A}_j$ is the value of final-state asymmetry of the j-th category, P_j represents the value of the corresponding three-dimensional probability density function (PDF), and $M^i_{\rm bc}$, ΔE^i, and $C'^i_{\rm NN}$ are the $M_{\rm bc}$, ΔE, and $C'_{\rm NN}$ values of the ith event, respectively.

With all the selection criteria applied, 98% of the signal MC events are correctly reconstructed while 2% are self-crossfeed (scf). In the fit, the ratio of scf to correctly reconstructed ("true") signal events is fixed. The signal yield ($N_{\rm sig}$) is the combined yield of the true signal and scf PDF. Five more event categories are included in the fit: continuum background, generic B background, $B^0 \to K^-K^+K^0_S$, $B^0 \to \pi^-\pi^+K^0_S$, and the remaining rare B background. The true signal PDF is described by the product of a sum of two Gaussian functions in $M_{\rm bc}$, a sum of three Gaussian functions in ΔE, and an asymmetric Gaussian function in $C'_{\rm NN}$. These PDF shapes are calibrated including possible data-MC differences obtained from the study of a high-statistics control mode $B^0 \to D^-\pi^+$, $D^- \to K^0_S\pi^-$. The continuum background PDF is given by the product of an ARGUS function [24] in $M_{\rm bc}$, a second-order polynomial in ΔE, and a sum of a Gaussian and an asymmetric Gaussian function in $C'_{\rm NN}$. All shape parameters of the continuum PDF are free in the fit, except for the ARGUS endpoint which is fixed to 5.2892 GeV/c^2. For the other contributions (scf, generic B, $B^0 \to K^-K^+K^0_S$, $B^0 \to \pi^-\pi^+K^0_S$, and rare B), their PDFs are described by a smoothed histogram in ΔE and $M_{\rm bc}$, and an asymmetric Gaussian function in $C'_{\rm NN}$ whose shape is based on MC. The yield of each category is floated. The $\mathcal{A}$ value is fixed to zero for all background categories.

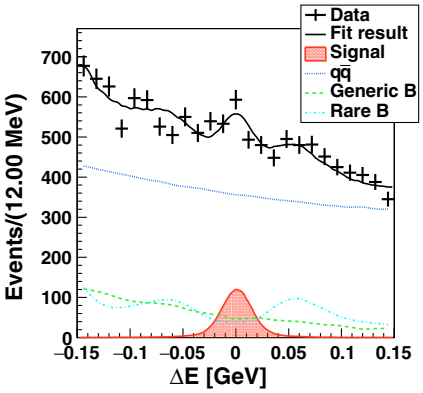

(a) ΔE

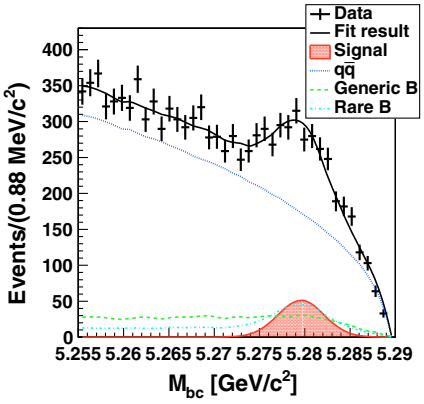

(b) $M_{\rm bc}$

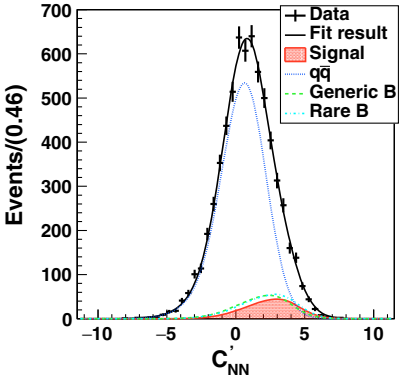

(c) C'_{NN}

FIG. 1. Signal-enhanced projections of the fit to $\bar{B}^0 \to K^0_S K^{\mp}\pi^{\pm}$ decays on ΔE, $M_{\rm bc}$, and $C'_{\rm NN}$. (a) ΔE in 5.272 GeV/c^2 $< M_{\rm bc} <$ 5.288 GeV/c^2 and $0 < C'_{\rm NN} < 5$. (b) $M_{\rm bc}$ in $|\Delta E| < 0.05$ GeV and $0 < C'_{\rm NN} < 5$. (c) $C'_{\rm NN}$ in $|\Delta E| < 0.05$ GeV and 5.272 GeV/c^2 $< M_{\rm bc} <$ 5.288 GeV/c^2.

The signal-enhanced projections of the fit are shown in Fig. 1. We obtain a signal yield of 490^{+46}_{-45} with a statistical significance of 13 standard deviations, and an $\mathcal{A}$ value of $(-8.5 \pm 8.9)\%$. The significance is defined as $\sqrt{-2\ln(\mathcal{L}_0/\mathcal{L}_{\rm max})}$, where $\mathcal{L}_0$ and $\mathcal{L}_{\rm max}$ are the likelihood values obtained by the fit with and without the signal yield fixed to zero, respectively.

The branching fraction is calculated using

$$\mathcal{B} = \frac{N_{\rm sig}}{\epsilon \times \eta \times N_{B\bar{B}}}, \tag{4}$$

where $N_{\rm sig}$, $N_{B\bar{B}}$, ϵ, and η are the fitted signal yield, the number of $B\bar{B}$ events ($= 772 \times 10^6$), the signal reconstruction efficiency, and the efficiency calibration factor, respectively. We assume that charged and neutral $B\bar{B}$ events are produced equally at the $\Upsilon(4S)$. The ϵ value

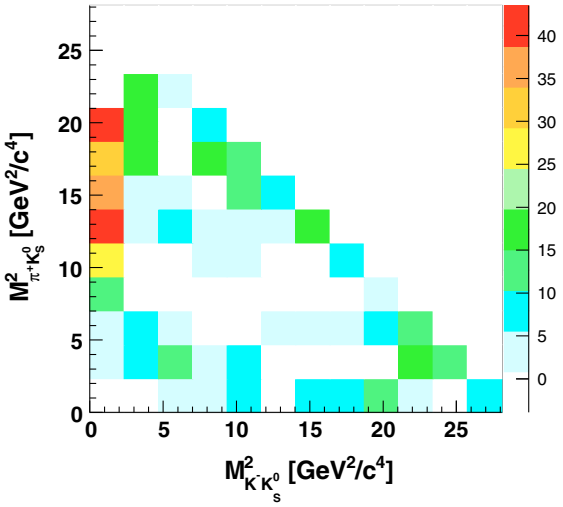

FIG. 2. Background-subtracted Dalitz plot of the $\bar{B}^0 \to K^0_S K^{\mp}\pi^{\pm}$ decays.

determined by MC, with all the selection criteria applied, is $(26.7 \pm 0.1)\%$. The calibration factor includes contributions due to various systematic effects $\eta = \eta_K \times \eta_\pi \times \eta_{\rm NN} \times \eta_{\rm fit}$, where $\eta_K (= 0.9948 \pm 0.0083)$ and $\eta_\pi (= 0.9512 \pm 0.0079)$ are the corrections due to $K^\pm$ and $\pi^\pm$ identification, and are obtained from a control sample of $D^{*+} \to D^0\pi^+$, $D^0 \to K^-\pi^+$. Similarly, $\eta_{\rm NN} (= 0.9897 \pm 0.0208)$ is due to the requirement on $C_{\rm NN}$ and is obtained from a sample of $B^0 \to D^-\pi^+$, $D^- \to K^0_S\pi^-$. The factor $\eta_{\rm fit} (= 1.022 \pm 0.004)$ is due to fit bias, obtained from an ensemble test on the fitter.

Figure 2 shows the background-subtracted Dalitz plot obtained with the ${}_s\mathcal{P}lot$ method. Structures around the regions $M^2_{K^-K^0_S} < 2\ {\rm GeV}^2/c^4$ and $7\ {\rm GeV}^2/c^4 < M^2_{\pi^+K^0_S} < 23\ {\rm GeV}^2/c^4$ are visible. We also obtain background-subtracted distributions after separating into five bins, and then calculate the differential branching fractions as functions of the three Dalitz variables with the yield and reconstruction efficiency within each bin. We use a similar binning scheme as the one in Ref. [9]. Figure 3 shows the

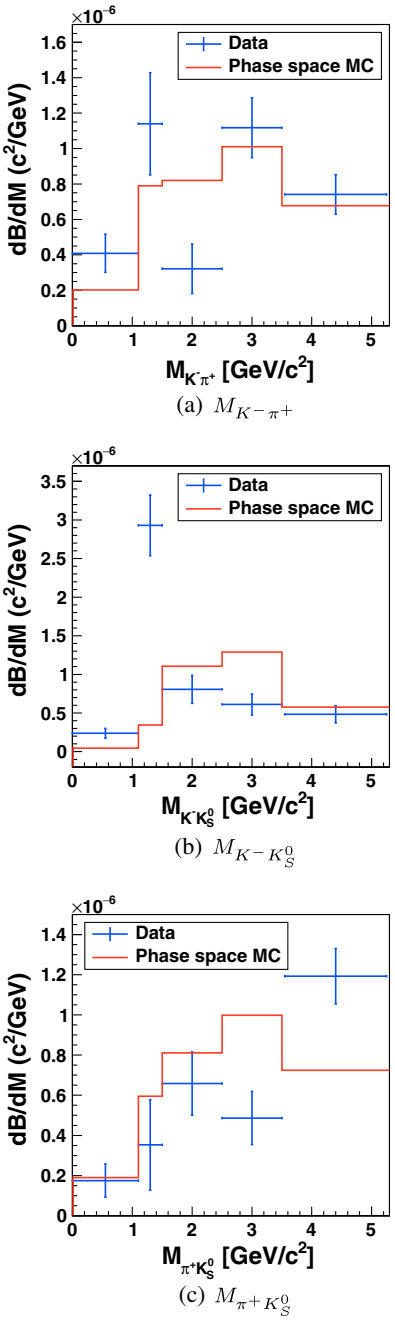

(a) $M_{K^-\pi^+}$

(b) $M_{K^-K^0_S}$

(c) $M_{\pi^+K^0_S}$

FIG. 3. Differential branching fraction as functions of Dalitz variables.

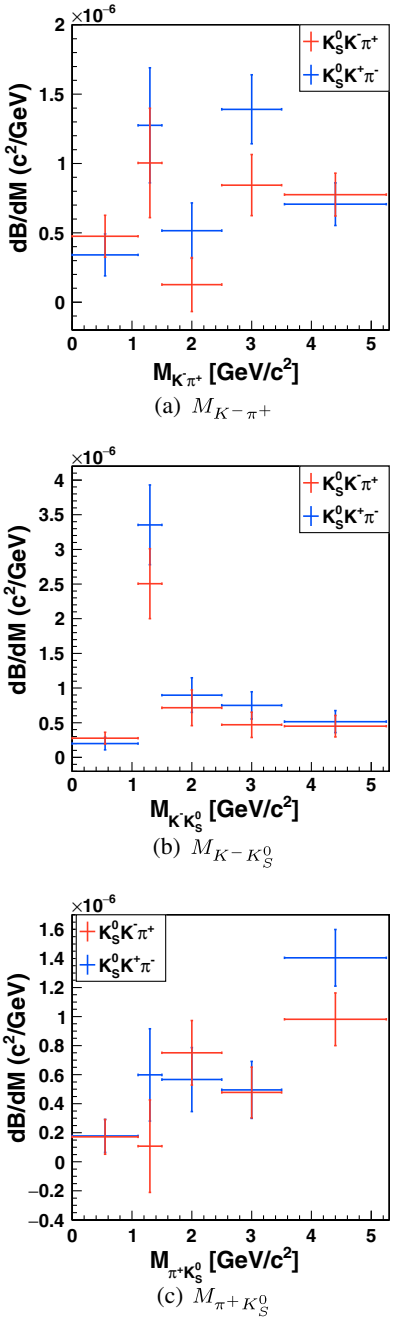

(a) $M_{K^-\pi^+}$

(b) $M_{K^-K^0_S}$

(c) $M_{\pi^+K^0_S}$

FIG. 4. Differential branching fraction as functions of the Dalitz variables for the two reconstructed B final states: $K^0_S K^-\pi^+$ (red points with error bars) and $K^0_S K^+\pi^-$ (blue points with error bars).

TABLE I. Signal yields, efficiency, and differential branching fraction in each $M_{K^-\pi^+}$, $M_{K^-K^0_S}$, and $M_{\pi^+K^0_S}$ bin.

				$K^0_SK^-\pi^+$	$K^0_SK^+\pi^-$	$K^0_SK^-\pi^+$	$K^0_SK^+\pi^-$
(c^2/GeV)	eff	Yield	$d\mathcal{B}/dM(10^{-7})$	yield	yield	$d\mathcal{B}/dM(10^{-7})$	$d\mathcal{B}/dM(10^{-7})$
$M_{K^-\pi^+}$							
0–1.1	0.301	$69.2 \pm 18.0 \pm 3.0$	$4.1 \pm 1.1 \pm 0.2$	$40.3 \pm 12.7 \pm 1.7$	$28.9 \pm 12.8 \pm 1.2$	$2.4 \pm 0.7 \pm 0.1$	$1.7 \pm 0.8 \pm 0.1$
1.1–1.5	0.306	$71.3 \pm 17.8 \pm 3.1$	$11.4 \pm 2.8 \pm 0.5$	$31.4 \pm 12.3 \pm 1.4$	$39.9 \pm 12.9 \pm 1.7$	$5.0 \pm 2.0 \pm 0.2$	$6.4 \pm 2.1 \pm 0.3$
1.5–2.5	0.289	$47.5 \pm 20.5 \pm 2.0$	$3.2 \pm 1.4 \pm 0.1$	$9.4 \pm 14.3 \pm 0.4$	$38.1 \pm 14.7 \pm 1.6$	$0.6 \pm 1.0 \pm 0.0$	$2.6 \pm 1.0 \pm 0.1$
2.5–3.5	0.262	$149.7 \pm 21.7 \pm 6.4$	$11.2 \pm 1.6 \pm 0.5$	$56.5 \pm 14.6 \pm 2.4$	$93.2 \pm 16.1 \pm 4.0$	$4.2 \pm 1.1 \pm 0.2$	$7.0 \pm 1.2 \pm 0.3$
> 3.5	0.237	$152.7 \pm 22.0 \pm 6.6$	$7.4 \pm 1.1 \pm 0.3$	$79.9 \pm 15.5 \pm 3.4$	$72.8 \pm 15.5 \pm 3.1$	$3.9 \pm 0.8 \pm 0.2$	$3.5 \pm 0.8 \pm 0.2$
$M_{\pi^+K^0_S}$							
0–1.1	0.275	$27.1 \pm 12.7 \pm 1.2$	$1.8 \pm 0.8 \pm 0.1$	$13.3 \pm 9.2 \pm 0.6$	$13.8 \pm 8.7 \pm 0.6$	$0.9 \pm 0.6 \pm 0.0$	$0.9 \pm 0.6 \pm 0.0$
1.1–1.5	0.269	$19.4 \pm 12.4 \pm 0.8$	$3.5 \pm 2.2 \pm 0.2$	$3.0 \pm 8.8 \pm 0.1$	$16.5 \pm 8.7 \pm 0.7$	$0.5 \pm 1.6 \pm 0.0$	$3.0 \pm 1.6 \pm 0.1$
1.5–2.5	0.252	$84.8 \pm 20.0 \pm 3.6$	$6.6 \pm 1.5 \pm 0.3$	$48.3 \pm 14.2 \pm 2.1$	$36.5 \pm 14.1 \pm 1.6$	$3.8 \pm 1.1 \pm 0.2$	$2.8 \pm 1.1 \pm 0.1$
2.5–3.5	0.264	$65.7 \pm 17.6 \pm 2.8$	$4.9 \pm 1.3 \pm 0.2$	$32.2 \pm 11.7 \pm 1.4$	$33.4 \pm 13.2 \pm 1.4$	$2.4 \pm 0.9 \pm 0.1$	$2.5 \pm 1.0 \pm 0.1$
> 3.5	0.283	$293.4 \pm 31.5 \pm 12.6$	$11.9 \pm 1.3 \pm 0.5$	$120.7 \pm 21.7 \pm 5.2$	$172.7 \pm 22.8 \pm 7.4$	$4.9 \pm 0.9 \pm 0.2$	$7.0 \pm 0.9 \pm 0.3$
$M_{K^-K^0_S}$							
0–1.1	0.245	$32.9 \pm 8.5 \pm 1.4$	$2.4 \pm 0.6 \pm 0.1$	$19.1 \pm 5.8 \pm 0.8$	$13.7 \pm 6.2 \pm 0.6$	$1.4 \pm 0.4 \pm 0.1$	$1.0 \pm 0.5 \pm 0.0$
1.1–1.5	0.258	$154.6 \pm 19.6 \pm 6.6$	$29.3 \pm 3.7 \pm 1.3$	$66.1 \pm 13.0 \pm 2.8$	$88.5 \pm 14.7 \pm 3.8$	$12.5 \pm 2.5 \pm 0.5$	$16.8 \pm 2.8 \pm 0.7$
1.5–2.5	0.235	$96.9 \pm 21.3 \pm 4.2$	$8.1 \pm 1.8 \pm 0.3$	$43.0 \pm 15.3 \pm 1.8$	$53.9 \pm 14.8 \pm 2.3$	$3.6 \pm 1.3 \pm 0.2$	$4.5 \pm 1.2 \pm 0.2$
2.5–3.5	0.267	$83.4 \pm 18.1 \pm 3.6$	$6.1 \pm 1.3 \pm 0.3$	$32.1 \pm 12.3 \pm 1.4$	$51.3 \pm 13.2 \pm 2.2$	$2.4 \pm 0.9 \pm 0.1$	$3.8 \pm 1.0 \pm 0.2$
> 3.5	0.292	$122.6 \pm 27.8 \pm 5.3$	$4.8 \pm 1.1 \pm 0.2$	$57.2 \pm 19.5 \pm 2.5$	$65.5 \pm 19.9 \pm 2.8$	$2.3 \pm 0.8 \pm 0.1$	$2.6 \pm 0.8 \pm 0.1$

differential branching fractions as functions of the three Dalitz variables including comparison to the MC with a three-body phase space model. Large deviations from phase space expectations are found around 1.2 GeV/c^2 in the $M_{K^-K^0_S}$ spectrum as well as near 3.0–4.2 GeV/c^2 in the $M_{\pi^+K^0_S}$ spectrum. No obvious structure is observed in the low-mass regions of both $M_{K^-\pi^+}$ and $M_{\pi^+K^0_S}$, which is consistent with previous two-body decay measurements [5,7,8].

Differential branching fractions are shown separately for the $K^0_SK^-\pi^+$ and $K^0_SK^+\pi^-$ final states in Fig. 4. Within each bin of the Dalitz variables, the results are consistent with no asymmetry. The details of the differential branching fraction calculation in each bin are summarized in Table I.

Various sources of systematic uncertainties in the branching fraction calculation are listed in Table II. The uncertainty due to the number of $B\bar{B}$ events is 1.4%. The uncertainty due to the charged-track reconstruction efficiency is estimated to be 0.35% per track by using partially reconstructed $D^{*+} \to D^0\pi^+$, $D^0 \to \pi^+\pi^-K^0_S$. The uncertainties due to $K^\pm$ and $\pi^\pm$ identification are obtained by the control sample study of $D^{*+} \to D^0\pi^+$, $D^0 \to K^-\pi^+$. The uncertainty due to the $K^0_S \to \pi^+\pi^-$ branching fraction is based on its world average [20]. The uncertainty due to K^0_S identification is estimated to be 1.6% based on a $D^{*+} \to D^0\pi^+$, $D^0 \to K^0_S\pi^0$ control sample [25]. The uncertainty due to continuum suppression with the requirement on C_{NN} is obtained from a control sample of $B^0 \to D^-\pi^+$, $D^- \to K^0_S\pi^-$. The uncertainty of the reconstruction efficiency is due to limited MC statistics. The uncertainty due to fixed PDF shapes is estimated by the deviation of fitted signal yield when varying the parameters of the PDFs in different cases. For all the smoothed histograms, we vary their binning parameters. For the PDFs with fixed parametrization, the fixed parameters are randomized by using a Gaussian random number to repeat data fits, and the uncertainty of the yield distribution is quoted. The uncertainty due to fit bias is obtained from an ensemble test on the fitter.

Various sources of systematic uncertainties in $\mathcal{A}$ are listed in Table III. The uncertainty due to $K^\pm$ and $\pi^\pm$

TABLE II. Summary of systematic uncertainties on the branching fraction.

Source	in %
$N_{B\bar{B}}$	1.4
Tracking	0.7
$K^\pm$ identification	0.8
$\pi^\pm$ identification	0.8
$\mathcal{B}(K^0_S \to \pi^+\pi^-)$	0.1
$K^0_S \to \pi^+\pi^-$ reconstruction	1.6
Continuum suppression	2.1
Limited MC statistics	0.1
Signal PDF	2.7
Background PDF	0.4
Fit bias	0.4
Total	4.3

TABLE III. Summary of systematic uncertainties on $\mathcal{A}$.

Source	in %
Detector bias	0.6
Signal PDF	2.7
Background PDF	0.9
Total	2.9

detection bias are obtained from the control samples of $D^+ \to \phi\pi^+$ and $D_s^+ \to \phi\pi^+$ [26], and $D^+ \to K_S^0\pi^+$ [27], respectively. The uncertainties due to the fixed PDF shapes are treated similarly to those on the branching fraction. They are estimated from the deviation of the fitted value of $\mathcal{A}$ with varying the conditions of those PDFs in different cases.

In summary, we have measured the branching fraction and asymmetry $\mathcal{A}$ of $\bar{B}^0 \to K_S^0 K^\mp \pi^\pm$ using a data sample of 711 fb^{-1} collected by Belle. We obtain a branching fraction of $(3.60 \pm 0.33 \pm 0.15) \times 10^{-6}$ and an $\mathcal{A}$ of $(-8.5 \pm 8.9 \pm 0.2)\%$, where the first uncertainty is statistical and the second is systematic. The measured $\mathcal{A}$ value is consistent with no asymmetry. Hints of peaking structures are seen in the regions $M^2_{K^-K_S^0} < 2$ GeV$^2/c^4$ and 7 GeV$^2/c^4 < M^2_{\pi^+K_S^0} < 23$ GeV$^2/c^4$ in the Dalitz plot. The peaking structure in $M^2_{K^-K_S^0}$ is consistent with the result from the previous $B^+ \to K^+K^-\pi^+$ measurement. A cross-check is performed by calculating the differential branching fraction after projecting onto each Dalitz variable, and hints of peaking structures are found near 1.2 GeV$/c^2$ in $M_{K^-K_S^0}$ and around 4.2 GeV$/c^2$ in $M_{\pi^+K_S^0}$ when compared to the phase space MC. No obvious K^* structure is seen in either low $M_{K^-\pi^+}$ or $M_{\pi^+K_S^0}$ spectra, which are consistent with the *BABAR* and LHCb results [5,7,8]. No localized final-state asymmetry is observed. In the near future, experiments with large data sets such as Belle II and LHCb can perform a more detailed analysis exploiting the full Dalitz plot.

ACKNOWLEDGMENTS

We thank the KEKB group for excellent operation of the accelerator; the KEK cryogenics group for efficient solenoid operations; and the KEK computer group, the NII, and PNNL/EMSL for valuable computing and SINET5 network support. We acknowledge support from MEXT, JSPS and Nagoya's the Tau-Lepton Physics Research Center (TLPRC) (Japan); ARC (Australia); FWF (Austria); NSFC and the Chinese Academy of Science Center for Excellence in Particle Physics (CCEPP) (China); MSMT (Czechia); the Carl Zeiss Foundation (CZF), DFG, the Excellence Cluster Universe (EXC153), and the VolkswagenStiftung (VS) (Germany); DST (India); INFN (Italy); MOE, MSIP, NRF, RSRI, Foreign Large-size Research Facility Application Supporting project (FLRFAS) project and GSDC of KISTI and Korea Research Environment Open Network (KREONET)/Global Ring Network for Advanced Application Development (GLORIAD) (Korea); MNiSW and NCN (Poland); Ministry of Science and Higher Education of the Russian Federation (MSHE), Grant No. 14.W03.31.0026 (Russia); ARRS (Slovenia); IKERBASQUE (Spain); SNSF (Switzerland); MOE and MOST (Taiwan); and DOE and NSF (USA).

[1] I. Bediaga, I. I. Bigi, A. Gomes, G. Guerrer, J. Miranda, and A. C. dosReis, Phys. Rev. D **80**, 096006 (2009).
[2] I. Bediaga, J. Miranda, A. C. dosReis, I. I. Bigi, A. Gomes, J. M. OtaloraGoicochea, and A. Veiga, Phys. Rev. D **86**, 036005 (2012).
[3] Throughout this paper, inclusion of charge-conjugate decay modes is implied unless otherwise stated.
[4] P. del Amo Sanchez *et al.* (*BABAR* Collaboration), Phys. Rev. D **82**, 031101 (2010).
[5] B. Aubert *et al.* (*BABAR* Collaboration), Phys. Rev. D **74**, 072008 (2006).
[6] R. Aaij *et al.* (LHCb Collaboration), J. High Energy Phys. 11 (2017) 027.
[7] R. Aaij *et al.* (LHCb Collaboration), New J. Phys. **16**, 123001 (2014).
[8] R. Aaij *et al.* (LHCb Collaboration), J. High Energy Phys. 01 (2016) 012.
[9] C.-L. Hsu *et al.* (Belle Collaboration), Phys. Rev. D **96**, 031101 (2017).
[10] B. Aubert *et al.* (*BABAR* Collaboration), Phys. Rev. Lett. **99**, 221801 (2007).
[11] R. Aaij *et al.* (LHCb Collaboration), Phys. Rev. Lett. **112**, 011801 (2014).
[12] R. Aaij *et al.* (LHCb Collaboration), Phys. Rev. D **90**, 112004 (2014).
[13] M. Pivk and F. R. Le Diberder, Nucl. Instrum. Methods Phys. Res., Sect. A **555**, 356 (2005).
[14] A. Abashian *et al.* (Belle Collaboration), Nucl. Instrum. Methods Phys. Res., Sect. A **479**, 117 (2002); also see detector section in J. Brodzicka *et al.*, Prog. Theor. Exp. Phys. **2012**, 04D001 (2012).

[15] S. Kurokawa and E. Kikutani, Nucl. Instrum. Methods Phys. Res., Sect. A **499**, 1 (2003), and other papers included in this volume; T. Abe *et al.*, Prog. Theor. Exp. Phys. **2013**, 03A001 (2013) and references therein.
[16] D. J. Lange, Nucl. Instrum. Methods Phys. Res., Sect. A **462**, 152 (2001).
[17] R. Brun *et al.*, CERN Report No. DD/EE/84-1, 1987.
[18] M. Feindt and U. Kerzel, Nucl. Instrum. Methods Phys. Res., Sect. A **559**, 190 (2006).
[19] H. Nakano, Ph.D. thesis, Tohoku University, 2014, Chap. 4, https://tohoku.repo.nii.ac.jp/?action=pages_view_main&active_action=repository_view_main_item_detail&item_id=70563&item_no=1&page_id=33&block_id=38.
[20] M. Tanabashi *et al.* (Particle Data Group), Phys. Rev. D **98**, 030001 (2018).
[21] R. A. Fisher, Annals of human genetics **7**, 179 (1936).
[22] G. C. Fox and S. Wolfram, Phys. Rev. Lett. **41**, 1581 (1978); The modified moments used in this paper are described in S. H. Lee *et al.* (Belle Collaboration), Phys. Rev. Lett. **91**, 261801 (2003).
[23] S. Brandt, C. Peyrou, R. Sosnowski, and A. Wroblewski, Phys. Lett. **12**, 57 (1964).
[24] H. Albrecht *et al.* (ARGUS Collaboration), Phys. Lett. B **241**, 278 (1990).
[25] N. Dash *et al.* (Belle Collaboration), Phys. Rev. Lett. **119**, 171801 (2017).
[26] M. Starič *et al.* (Belle Collaboration), Phys. Rev. Lett. **108**, 071801 (2012).
[27] B. R. Ko *et al.* (Belle Collaboration), Phys. Rev. Lett. **109**, 021601 (2012).